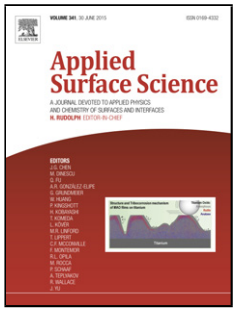

Title: Corrosion performance of ZrN/ZrO_2 multilayer coatings deposited on 304 stainless steel using multi-arc ion plating

Authors: Zhefeng Lei, Qingqing Zhang, Xiaodong Zhu, Dayan Ma, Fei Ma, Zhongxiao Song, Yong Qing Fu

PII: S0169-4332(17)31928-1
DOI: http://dx.doi.org/doi:10.1016/j.apsusc.2017.06.273
Reference: APSUSC 36473

To appear in: *APSUSC*

Received date: 29-3-2017
Revised date: 22-6-2017
Accepted date: 26-6-2017

Please cite this article as: Zhefeng Lei, Qingqing Zhang, Xiaodong Zhu, Dayan Ma, Fei Ma, Zhongxiao Song, Yong Qing Fu, Corrosion performance of ZrN/ZrO2 multilayer coatings deposited on 304 stainless steel using multi-arc ion plating, Applied Surface Sciencehttp://dx.doi.org/10.1016/j.apsusc.2017.06.273

Corrosion performance of ZrN/ZrO_2 multilayer coatings deposited on 304 stainless steel using multi-arc ion plating

Zhefeng Lei[1,2], Qingqing Zhang[1], Xiaodong Zhu[1], Dayan Ma[1], Fei Ma[1], Zhongxiao Song[1*], Yong Qing Fu[2,*]

1. State Key Laboratory for Mechanical Behavior of Materials, School of Materials Science and Engineering, Xi'an Jiaotong University, Xi'an, Shaanxi 710049, China

2. Faculty of Engineering and Environment, Northumbria University, Newcastle upon Tyne, NE1 8ST, UK

Highlights:

- A optimized process parameters for depositing the zirconia coating were being developed by using multi arc ion plating technique.
- A ZrN/ZrO2 multilayer specimen that possesses symmetrical structure (thickness of each sublayers: 345 nm) and a suitable modulation ratio (1:1) showing excellent toughness and corrosion resistance properties.
- Multilayer structure has integrated the advantages of the sub-layers in toughness and corrosion resistance, and the interfaces should blocked the diffusion path of the cracks during serviced in a

*Corresponding author. Zhongxiao Song, E-mail: ZhongxiaoSong@mail.xjtu.edu.cn; Yong Qing Fu, richard.fu@northumbria.ac.uk

demanding environment.

Abstract

Coatings of single-layer ZrN, bilayer and multilayer ZrN/ZrO_2 were deposited onto 304 stainless steel using a multi-arc ion plating technique, and their corrosion properties were tested in various solutions of 3.5 wt% sodium chloride (NaCl), 10 wt% and 20 wt% hydrochloric (HCl) acids, respectively. Results showed that the single-layer ZrN coating resisted the corrosion in the HCl acid with a concentration of 10 wt%, and the multilayer ZrN/ZrO_2 coating acted as an effective protective layer in 20 wt% HCl solution. Polarization curve of the bilayer ZrN/ZrO_2 coated specimens showed the lowest corrosion current density in 3.5 wt% NaCl and 20 wt% HCl solutions. However after polarization tests, the bilayer coating showed severe delamination after exposed in air, due to the large coating stress and brittleness of oxide ceramic layer. The multilayer ZrN/ZrO_2 coating exhibited similar corrosion potentials and corrosion current densities compared with those of the bilayer coating. However, there was hardly any microscopic failure observed on the surfaces of the multilayer coatings after tested in all chloride solutions, which is attributed to the combined effects including improvement in coating toughness due to the multilayer design and ZrN sub-layer, reduced coating stress, and good corrosion resistance from the ZrO_2 sub layer.

Keywords:

ZrO_2, multilayer, electrochemical corrosion, polarization curve,

1. Introduction

Type 304 stainless steel (304 SS) is one of the most widely used chrome-nickel SS because of its good corrosion resistance, heat resistance, mechanical and machinable properties. However, when it is used in an environment containing chloride ions, several corrosion related phenomena such as stress induced corrosion, pitting corrosion and intergranular corrosion often occur, and it is well known that the chloride ions are commonly existed in salt, sweat, sea water and soil. In recent years, research has been focused on solving the above problems using various types of coatings, such as TiN [1], ZrN [2], TiAlN [3], TiSiN [4], ZrO_2 [5], Ti/TiN [6], CrN/TiN [7], TiN/TiAlN [8]. Among these coatings, ZrN has an outstanding anti-corrosion property, and zirconium metal possesses a high melting point and a good corrosion resistance. This is critical because during deposition of nitride or oxide coatings using metallic targets, the existence of metal particles in the coating due to the fast deposition is inevitable, thus the corrosion resistance of the coating will be affected by these metallic particles.

Whereas for ZrN, its corrosion resistance in a harsh environment such as in a concentrated hydrochloric acid is generally not as good as oxide ceramics [5, 9]. For ZrN coating, oxygen is easily absorbed on its surface thus the surface is commonly covered by a layer of ZrO_2 [2]. Zirconia is an important ceramic material for industry

applications due to its wide band gap and thermal stability, the latter of which is attractive to be used as a coating for stainless steel [10]. In addition, for a better corrosion resistance, the coatings with bilayer or multilayer architectures are commonly used and show a better performance than single layer coating [11, 12]. Based on this, we proposed that the ZrO_2/ZrN multilayered coatings should be a strong corrosion-resistant coating for the 304 SS.

Currently, several techniques are commonly used to deposit ZrO_2 coating on SS surfaces: sol–gel deposition [13], hydrothermal process [10], pulsed laser deposition [14], chemical vapor deposition [15], ultrasonic spray pyrolysis-nitriding and magnetron sputtering technique [5]. Whereas ZrN coating with a compact structure of face center cubic (FCC) and smooth surface for a good corrosion resistance were mostly deposited using physical vapor deposition (PVD) techniques [16]. Among these methods, multi-arc ion plating technique (MAIP) [17, 18] is widely used in industrial production due to its high deposition rate and good interfacial bond strength between film and substrate. Therefore, optimising the process parameters of MAIP to achieve a rapid deposition of zirconia coating is of great significance.

In this study, single-layer ZrN, bilayer and multilayer ZrN/ZrO_2 coatings were deposited using the MAIP. All the coating samples were characterized using X-ray diffraction (XRD), scanning electron microscope (SEM) and X-ray photoelectron spectroscopy (XPS). Their corrosion resistance properties were evaluated using a potentiodynamic polarization method in different chloride ion media including 3.5 wt% NaCl, 10 wt% HCl and 20 wt% HCl solutions, respectively.

2. Experimental details

Commercial stainless steel sheets (304 SS) were used as the substrate. Before deposition, the 304 SS substrates of 15×15×3 mm^3 in size were cleaned in an ultrasonic bath with acetone and ethanol for 10 min, respectively, then plasma-cleaned in a deposition chamber using a bias voltage of 800 V in an argon plasma. Single layer ZrN, bilayer ZrN/ZrO_2 and multilayer ZrN/ZrO_2 coatings were deposited onto the substrates using the MAIP. TiAl alloy target (50 at.% of aluminum and 50 at.% of titanium) and zirconium target both of 62 mm in diameter were arranged on a cylindrical chamber wall (700 mm in height and 900 mm in diameter). The substrates were mounted onto a rotational holder at the center of the chamber. The minimum separation between the target and substrate was 300 mm, and the holder was rotated at a speed of 7 rpm. The deposition was conducted under a negative bias of -100 V with a duty cycle of 30% at 573 K, and the deposition pressure was 1.2~1.7 Pa. The DC arc sources were operated at 80 A, 17.3 V for TiAl target and 90 A, 22.4V for Zr target. During the deposition, the working gas was a mixture of argon and nitrogen for ZrN (whereas argon and oxygen for ZrO_2), and the flow rates of Ar, N_2 and O_2 were 12, 80 sccm and 70 sccm, respectively. In order to improve the coating adhesion, a 50 nm TiAl buffer layer was deposited before the nitride or oxide coatings. Some key deposition parameters are listed in Table 1.

Optical microscope and SEM (FEI Quanta 600 FEG) were used to characterize the surface and cross-section morphologies. XRD with a Cu Kα radiation (wavelength

of 0.15418 nm and voltage/current of 40kV/40mA) was used to analyze the crystalline phases of the multilayer ZrN/ZrO_2 specimen, and grazing-incidence XRD (GIXRD) was used to analyze the single layer ZrN and bilayer ZrN/ZrO_2 specimens. XPS (ESCALAB 250Xi, Thermo Fisher) with Al Kα X-ray source was used to analyze the elements and their chemical states in the coatings. The mechanical properties were characterized using an acoustic emission automatic scratch tester (WS-2005).

Electrochemical experiments were conducted using an Autolab (PGSTAT 128N) station. The coated specimens with a surface area of 1 cm^2 were adopted as the working electrode. Graphite rod and saturated calomel electrode were used as counter and reference electrodes, respectively. Prior to the beginning of the polarization procedures, the specimens were submerged for 60 minutes in order to establish the free corrosion potential (E_{corr}) [19, 20]. A linear sweep voltammetry with a scanning rate of 5 mV/s [21, 22] was applied in three types of chloride electrolyte solutions: 3.5 wt% NaCl, 10 wt% and 20 wt% hydrochloric acid.

3. Results and Discussion

3.1. Coating characterization

Cross-sectional SEM images of the deposited coatings are shown in Fig. 1, and the measured film thickness values are listed in Table 1. The thickness of the ZrN single layer coating is about 4.8 μm (60 minute deposition). Here the thickness of the ZrN coating is optimized for its mechanical property and is also thick enough to

evaluate the corrosion resistance using the potentiodynamic polarization method. The surface elemental composition was obtained from XPS analysis: Zr-46.2 at%, N-21.9 at% and O-31.9 at%. Results confirmed that there is an oxide top-layer covered on the surface of ZrN coating due to the reactive nature of ZrN and surface adsorption [2].

The bilayer coating is formed by 3.2 μm thick ZrN (40 minute deposition) and 3.8 μm thick ZrO_2 (50 minute deposition), the elemental composition of ZrO_2 layer obtained from XPS analysis is: Zr-32.1 at% and O-67.9 at%. SEM analysis of film thickness confirmed that the deposition rates of both the ZrN and ZrO_2 sub-layers were ~80 nm/min.

The multilayer coating structures shown in Fig. 1c clearly reveal the distinct interfaces and dense structures of each sub-layer with an interface density of 1/345 nm^{-1} (345 nm thick for each sub-layer). The deposition rates of each sub-layer in the multilayer coating are slightly lower than those of the continuous deposition samples (i.e. single layer and bilayer coatings). For the MAIP process, the deposition rate is related to the chamber temperature and interface status (epitaxial growth or not) of each sub-layer. During the continuous deposition, the chamber temperature was increased slowly from 300 ℃ to 350 ℃ for the unremitting thermal radiation from the target surface, whereas it was kept at 300 ℃ during the multilayer coating deposition process. Furthermore, interface pinning/interface mixing [23, 24] will happen at the interfaces of ZrN and ZrO_2 sub-layers, thus resulting in denser microstructures and lower deposition rates than the continuous deposition specimens.

XRD patterns of the samples are shown in Fig. 2. The single-layer ZrN coating

shows an FCC structure with a lattice constant of 4.574 Å. The ZrO_2 top-layer of bilayer sample has a mixture of monoclinic structure (a=5.17 Å, b=5.26 Å, c=5.30 Å) and a minor cubic structure (a=5.07 Å). Compared with XRD PDF card (No. 5-543, m-ZrO_2), both the peaks of ZrO_2 (111) at 2θ=28.3° and ZrO_2 (-111) at 2θ=31.57° are shifted to the right-hand side from 2θ=28.05° and 2θ=31.38°, indicating the residual compressive stress exists in the ZrO_2 top-layer which was continuously deposited using the MAIP. The multilayer coating shows a superimposition of diffraction peaks from ZrN and ZrO_2 and minor peaks from the stainless steel substrate. As the X-ray beam penetrates through the whole thickness of coating, we can conclude that the multilayer coating has minor intermixing interfaces between ZrN sub-layers and ZrO_2 sub-layers as there were no new peaks (or new phases) detected.

From XPS spectra of Zr-3d shown in Fig. 3, there are some apparent differences in the Zr states. The Zr-N bond at 179.9 eV (Fig. 3-a) correspond to an unsaturated covalent compound ZrN_x (x≈0.68), the element N is easily to be replaced by element O, so the N (or O) within the interface of ZrN sub-layer and ZrO_2 sub-layer should be a graded distribution which can strengthen the interfacial bonding of sub-layers. From the Zr-3d spectra of ZrO_2 top-layer for bilayer specimen (Fig. 3-b), the three peaks at 185.8 eV, 183.4 eV and 180.7 eV are corresponding to ZrO_2 (3d-3/2), ZrO_2 (3d-5/2) and ZrO_x (3d-5/2) respectively. The small peak at 179 eV corresponds to metallic state of Zr (3d-5/2), which only accounts for approximately 2 percentage and can be attributed to the metal droplets generated during deposition process when using MAIP technique.

The scratched morphology and the corresponding acoustic emission spectra are displayed in Fig. 4. The critical loads for the single layer ZrN, bilayer ZrN/ZrO_2, multilayer ZrN/ZrO_2 correspond to scale flaking are 48 N, 15 N, 38 N, respectively. [25] The bilayer specimen shows a serious peeling-off on both sides of the scratch mark, and that of single layer ZrN specimen is flat and smooth. The multilayer sample has a good bond strength of 38 N which is higher than that of bilayer sample, and the scratch morphology is similar to that of single-layer ZrN. Obviously, the brittleness of oxide ZrO_2 is higher than that of nitride ZrN. Therefore, the good design of multilayer structure (i.e., the ratio of thickness for each sub-layer was 1:1) not only reduces the film stress from interfaces effectively, but also integrates the toughnesss of ZrN sub-layer into the multilayer system, which results in satisfactory mechanical properties.

3.2. Corrosion resistance

The electrochemical performance of coated 304 SS was investigated using potentiodynamic polarization measurements in different chloride solutions. Fig. 5 shows the curves of linear polarization for the coating specimens tested in 3.5 wt% NaCl solution, and the curve of uncoated 304SS is also shown for comparisons. The obtained values of corrosion potential E_{corr} and corrosion current density I_{corr} of all coated samples are listed in Table 2, and they are clearly lower than those of uncoated stainless steel. For the potentiodynamic polarization curve, I_{corr} is the critical parameter for evaluating the corrosion resistance of materials, and the lower this value,

the better corrosion resistance (supposing the parameter of E_{corr} does not change significantly). From both Fig. 5 and Table 2, the bilayer and multilayer coatings have much lower I_{corr} values than those of ZrN coated sample (i.e., I_{corr}=140, 4.2, 17 $nA \cdot cm^{-2}$ for ZrN, bilayer and multilayer coatings, respectively). This clearly reveals that the ZrO_2 exhibits a good corrosion resistance in the 3.5 wt% NaCl solution, which has previously been reported in literature [9, 21]. All the values of E_{corr} in 3.5 wt% NaCl (listed in Table 2) are very close to each other and have minor changes (from 0.335V to 0.401V).

Detailed studies of the surface morphology of the samples after potentiodynamic polarization tests showed apparent differences (see the first column in Fig .8). All the tested samples were washed with DI water, and exposed in air for observation. The ZrO_2 in the bilayer coating was found to peel-off totally with only discontinuous ZrN layer left on the surface after exposed for 3 hours as shown in image b-1 (Fig.8). Compared with the polarization curve in Fig. 5, the anode polarization current for the bilayer sample was rapidly increased to the similar value of the 304 SS at 0.02 V, indicating that the corrosive medium reached the surface of the substrate during the corrosion tests. This proves that the ZrO_2 layer is fragile with large stress. On the contrary, the surfaces of ZrN coating and multilayer coatings after corrosion tests and then exposed for a few days were similar to those before testing, and that of uncoated 304SS showed several spots which indicate the pitting corrosion was occurred during the test.

Figure 6 shows the potentiodynamic polarization curves of all specimens tested

in 10 wt% hydrochloric acid solution, and the obtained values of I_{corr} and E_{corr} are listed in Table 2. For tests with 10 wt% HCl, all the coated samples exhibit lower absolute values of corrosion potentials than those of the uncoated 304 SS (i.e., E_{corr} = -0.402, -0.407, -0.306, -0.335 V for SS, ZrN, bilayer and multilayer coatings, respectively). The I_{corr} values of the multilayer specimen are the lowest ones during the whole processes of cathode and anode polarization, and a non-smooth curve in anode polarization process (from -0.2V to 0.35V) was observed indicating that the corrosion exhibits an active-passive-transpassive behavior [22, 26] in the anodic region of the Tafel curves.

Surface morphologies of all the samples after polarization tests in 10 wt% HCl are shown in the second column of Fig. 8 (in which a-2, b-2, c-2 and S-2 are for ZrN, bilayer, multilayer coated samples and uncoated 304SS, respectively). The bilayer coating peels off from the substrate and only some ZrN debris are left on the surface after exposed for 3 hours as shown in image b-2 (Fig.8). For the ZrN single layer and ZrN/ZrO_2 multilayer samples, the images a-2 and c-2 clearly show that there are no apparent damages in the surface morphology. For the 304 SS substrate, a similar pitting corrosion morphology but with a darker surface color is observed in image S-2 compared with image S-1, indicating that the 304SS suffers more severe corrosion during the process than that tested in 3.5 wt% NaCl.

The potentiodynamic polarization curves for the specimens that were tested in the concentrated hydrochloric acid with a concentration of 6.02 mol/L (20 wt%) are shown in Fig. 7. Both the bilayer and multilayer ZrN/ZrO_2 coated specimens show a

lower corrosion current density I_{corr} and a lower absolute corrosion potential E_{corr} values than those of ZrN coated specimen and uncoated 304 SS, although the I_{corr} values are much higher than those tested in the lower concentration (10 wt%) HCl solution. A double-peak pattern is observed in the polarization curve of the multilayer specimen as shown in Fig. 7, in which the second peak is very close to the E_{corr} value with a potential of -0.355 V at the beginning of anodic polarization process. The formation of this double-peak pattern can be explained as follows.

In theory, ZrO_2 is an amphoteric oxide which becomes reactive under conditions of strong acid or strong alkaline. In addition, because it was deposited using the PVD method, the crystallization of ZrO_2 coating is not as good as those from the sintered ceramics. In the concentrated hydrochloric acid solution, the metastable zirconia is gradually eroded into a complex-ion based $ZrCl_6^{2-}$. During the following cathode and anode polarization processes, the polarization reactions of the ZrO_2 coating [5] can be listed as below:

Cathode polarization: $ZrO_2+4H^+ == Zr^{4+}+2H_2O$ (1)

Anode polarization: $ZrO_2+2Cl^- == ZrOCl_2 + O^{2-}$ (2)

$ZrOCl_2+4Cl^- == ZrCl_6^{2-}+O^{2-}$ (3)

In the concentrated hydrochloric solution, the cathode region of Tafel curve of multilayer coating is smooth indicating that no other corrosion reactions occur, and equation 1 would be the only polarization reaction. The reaction product at the beginning of anode polarization process ($ZrOCl_2$) could be further crystallized into a solid state and then attached to the surface of ZrO_2 top-layer. This will result in

another cathodic polarization reaction as below:

$$ZrOCl_2+2H^+==Zr^{4+}+2Cl^-+H_2O \quad (4)$$

The anode polarization process should be divided into three stages: i.e., (1) -0.382 V ~ -0.369 V (-0.369 V is the inflection point between -0.382 V and -0.355 V, and the main reaction should be anode polarization equation 2); (2) -0.369 V ~ -0.355 V (in which the main reaction should be cathodic polarization equation 4); (3) -0.355V ~ 0.35 V (in which the reaction should be cathodic polarization equations 2 and 3).

From the surface morphologies of specimens after tested in 20 wt% HCl solution (the third column in Fig. 8), image a-3 shows corrosion pits with a scale of 0.01 mm^2 and the color is darker than image a-1 and image a-2. These indicate that some chlorides are adsorbed on the surface. Image b-3 shows a similar phenomenon as in image b-2, which means that the coatings are peeled-off totally from the surface of 304SS. This indicates that the corrosion process occurs on the whole coating surface.

As the I_{corr} value of bilayer ZrN/ZrO_2 sample is lower than that of multilayer sample, so the terrible surface morphology should indicated a different corrosion process. The corrosion behavior of the bilayer sample tested in HCl solutions can be summarized as follows: (1) some corrosion pits are produced on the surface of ZrO_2 top-layer firstly; (2) whereafter, the pits act as the starting point for crack formation; (3) then the cracks penetrate into the films along columnar grain boundaries of the oxide coating and further propagate into the beneath ZrN layer; (4) Finally, polarization reaction occurs within the buffer layer and 304 SS substrate. Image c-3

(Fig.8) displays a well-reserved surface morphology of the multilayer ZrN/ZrO_2 coating after corrosion tests, indicating that it has an excellent corrosion resistance in 20 wt% HCl solution. Comparatively, the bilayer coating was peeling off of the 304SS (see image b-3) and the uncoated 304SS (see image S-3) was seriously corroded after the test.

4. Conclusions

Based on the commercial production technology of hard coatings such as TiN, CrN, ZrN etc., a preparation technology has been exploited to deposit the corrosion resistance ZrO_2 coating. Results showed that a multilayer ZrN/ZrO_2 coating with an interphase density of 1/345 nm^{-1} were successfully obtained.

The corrosion resistance of single layer ZrN, bilayer ZrN/ZrO_2 and multilayer ZrN/ZrO_2 coated 304 stainless steel were investigated in different chloride solutions such as 3.5 wt% NaCl, 10 wt% and 20% HCl. Results showed that the single layer ZrN coating withstand the corrosion in 3.5 wt% NaCl and 10 wt% HCl solutions. The bilayer ZrN/ZrO_2 specimen exhibited the lowest corrosion current density in 3.5 wt% NaCl and 20 wt% HCl solutions due to the ZrO_2 top-layer. However, serious peeling-off of coatings was observed after all the corrosion tests, mainly due to the large coating stress and the brittleness of oxide ceramics. The multilayer ZrN/ZrO_2 coating successfully protected the 304 SS in a highly harsh environment (tested in 20 wt% concentrated hydrochloric acid solution). The reasons are (1) the multilayer structure with a uniform thickness for each sub-layer reduces the large stress in

coating; (2) the interfaces should block the propagation paths of the cracks. The multilayer coating has a combined enhancement effects from the toughness of ZrN sub-layer and the corrosion resistance of ZrO_2 sub-layer, thus promising as the protective coating for 304 stainless steel.

Acknowledgements

This work was supported by the National Natural Science Foundation of China (NSFC Grant No. 51071119, 51101081, 51271139, 51471130, 51371136), Fundamental Research Funds for the Central Universities, and Newton Mobility Grant (IE161019) through Royal Society and NFSC, and Royal academy of Engineering UK-Research Exchange with China and India.

References

[1] A. Bahri, E. Kaçar, S.S. Akkaya, K. Elleuch, M. Ürgen, Wear protection potential of TiN coatings for 304 stainless steels used in rotating parts during olive oil extraction, Surface and Coatings Technology, 304 (2016) 560-566.
[2] R. Brown, M.N. Alias, R. Fontana, Effect of composition and thickness on corrosion behavior of TiN and ZrN thin films, Surface and Coatings Technology, 62 (1993) 467-473.
[3] S. Korablov, M.A.M. Ibrahim, M. Yoshimura, Hydrothermal corrosion of TiAlN and CrN PVD films on stainless steel, Corrosion Science, 47 (2005) 1839-1854.
[4] Q. Wan, H. Ding, M.I. Yousaf, Y.M. Chen, H.D. Liu, L. Hu, B. Yang, Corrosion behaviors of TiN and Ti-Si-N (with 2.9 at.% and 5.0 at.% Si) coatings by electrochemical impedance spectroscopy, Thin Solid Films, 616 (2016) 601-607.
[5] G.I. Cubillos, M. Bethencourt, J.J. Olaya, Corrosion resistance of zirconium oxynitride coatings deposited via DC unbalanced magnetron sputtering and spray pyrolysis-nitriding, Applied Surface Science, 327 (2015) 288-295.
[6] L. Chenglong, Y. Dazhi, L. Guoqiang, Q. Min, Corrosion resistance and hemocompatibility of multilayered Ti/TiN-coated surgical AISI 316L stainless steel, Materials Letters, 59 (2005) 3813-3819.
[7] Y.X. Ou, J. Lin, S. Tong, H.L. Che, W.D. Sproul, M.K. Lei, Wear and corrosion resistance of CrN/TiN superlattice coatings deposited by a combined deep oscillation magnetron sputtering and pulsed dc magnetron sputtering, Applied Surface Science, 351 (2015) 332-343.
[8] A.P. Kulkarni, V.G. Sargade, Characterization and Performance of AlTiN, AlTiCrN, TiN/TiAlN PVD Coated Carbide Tools While Turning SS 304, Materials and Manufacturing Processes, 30 (2015) 748-755.
[9] E. Ariza, L.A. Rocha, F. Vaz, L. Cunha, S.C. Ferreira, P. Carvalho, L. Rebouta, E. Alves, P. Goudeau, J.P. Rivière, Corrosion resistance of ZrNxOy thin films obtained by rf reactive magnetron sputtering, Thin Solid Films, 469-470 (2004) 274-281.
[10] N. Garg, S. Bera, G. Mangamma, V.K. Mittal, R. Krishnan, S. Velmurugan, Study of Fe2O3-ZrO2 interface of ZrO2 coating grown by hydrothermal process on stainless steel, Surface and Coatings Technology, 258 (2014) 597-604.
[11] E. Alat, A.T. Motta, R.J. Comstock, J.M. Partezana, D.E. Wolfe, Multilayer (TiN, TiAlN) ceramic coatings for nuclear fuel cladding, Journal of Nuclear Materials, 478 (2016) 236-244.
[12] H. Zhang, G. Lin, M. Hou, L. Hu, Z. Han, Y. Fu, Z. Shao, B. Yi, CrN/Cr multilayer coating on 316L stainless steel as bipolar plates for proton exchange membrane fuel cells, Journal of Power Sources, 198 (2012) 176-181.
[13] H.M. Abd El-Lateef, M.M. Khalaf, Corrosion resistance of ZrO2–TiO2 nanocomposite multilayer thin films coated on carbon steel in hydrochloric acid solution, Materials Characterization, 108 (2015) 29-41.
[14] K. Rodrigo, J. Knudsen, N. Pryds, J. Schou, S. Linderoth, Characterization of yttria-stabilized zirconia thin films grown by pulsed laser deposition (PLD) on various substrates, Applied Surface Science, 254 (2007) 1338-1342.
[15] J.R.V. Garcia, T. Goto, Thermal barrier coatings produced by chemical vapor deposition, Science and Technology of Advanced Materials, 4 (2016) 397-402.
[16] Y.-Y. Chang, C.-J. Wu, Mechanical properties and impact resistance of multilayered TiAlN/ZrN coatings, Surface and Coatings Technology, 231 (2013) 62-66.

[17] D. Zhang, L. Duan, L. Guo, Z. Wang, J. Zhao, W.-H. Tuan, K. Niihara, TiN-coated titanium as the bipolar plate for PEMFC by multi-arc ion plating, International Journal of Hydrogen Energy, 36 (2011) 9155-9161.
[18] C.-H. Hsu, C.-Y. Lee, C.-C. Lee, Analysis on the corrosion behavior of DC53 tool steel coated by Ti–Al–C–N films via filtered cathodic arc deposition, Thin Solid Films, 517 (2009) 5212-5215.
[19] R.M. Souto, H. Alanyali, Electrochemical characteristics of steel coated with TiN and TiAlN coatings, Corrosion Science, 42 (2000) 2201-2211.
[20] W. Hu, J. Xu, X. Lu, D. Hu, H. Tao, P. Munroe, Z.-H. Xie, Corrosion and wear behaviours of a reactive-sputter-deposited Ta2O5 nanoceramic coating, Applied Surface Science, 368 (2016) 177-190.
[21] M.A.M. Ibrahim, S.F. Korablov, M. Yoshimura, Corrosion of stainless steel coated with TiN, (TiAl)N and CrN in aqueous environments, Corrosion Science, 44 (2002) 815-828.
[22] H. Zhang, L. Liu, J. Bai, X. Liu, Corrosion behavior and microstructure of electrodeposited nano-layered Ni–Cr coatings, Thin Solid Films, 595 (2015) 36-40.
[23] C.-K. Lin, C.-H. Hsu, Y.-H. Cheng, K.-L. Ou, S.-L. Lee, A study on the corrosion and erosion behavior of electroless nickel and TiAlN/ZrN duplex coatings on ductile iron, Applied Surface Science, 324 (2015) 13-19.
[24] P. Ren, S. Zhu, F. Wang, Microstructure and oxidation behavior of a Ni+CrAlYSiHfN/AlN multilayer coating fabricated by reactive magnetron sputtering, Corrosion Science, 104 (2016) 197-206.
[25] Z. Lei, Y. Liu, F. Ma, Z. Song, Y. Li, Oxidation resistance of TiAlN/ZrN multilayer coatings, Vacuum, 127 (2016) 22-29.
[26] V.B. Singh, A. Gupta, Active, passive and transpassive dissolution of In-718 alloy in acidic solutions, Materials Chemistry and Physics, 85 (2004) 12-19.

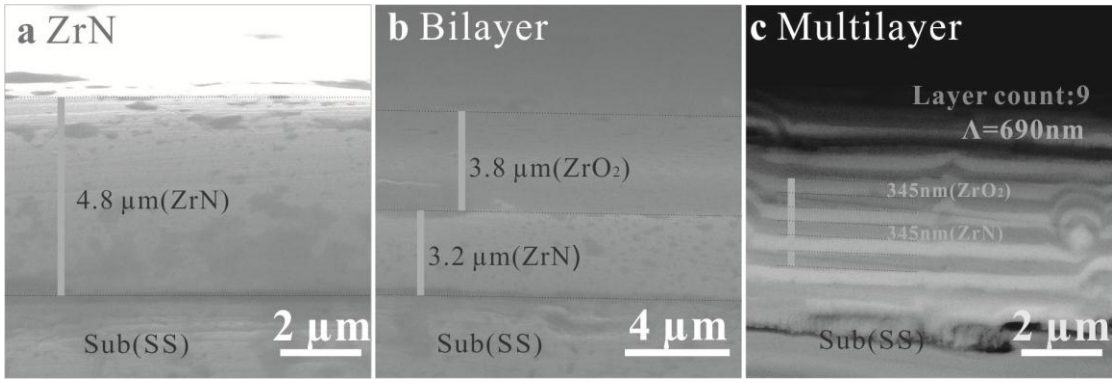

Fig. 1. Cross-sectional SEM images of (a) ZrN, (b) ZrN/ZrO_2 Bilayer, and (c) ZrN/ZrO_2 Multilayer.

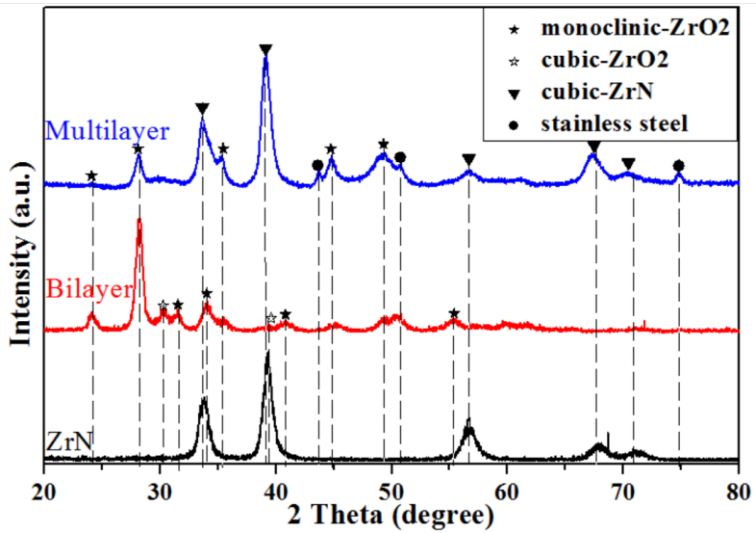

Fig.2. XRD patterns of ZrN, Bilayer and Multilayer ZrN/ZrO_2 coatings.

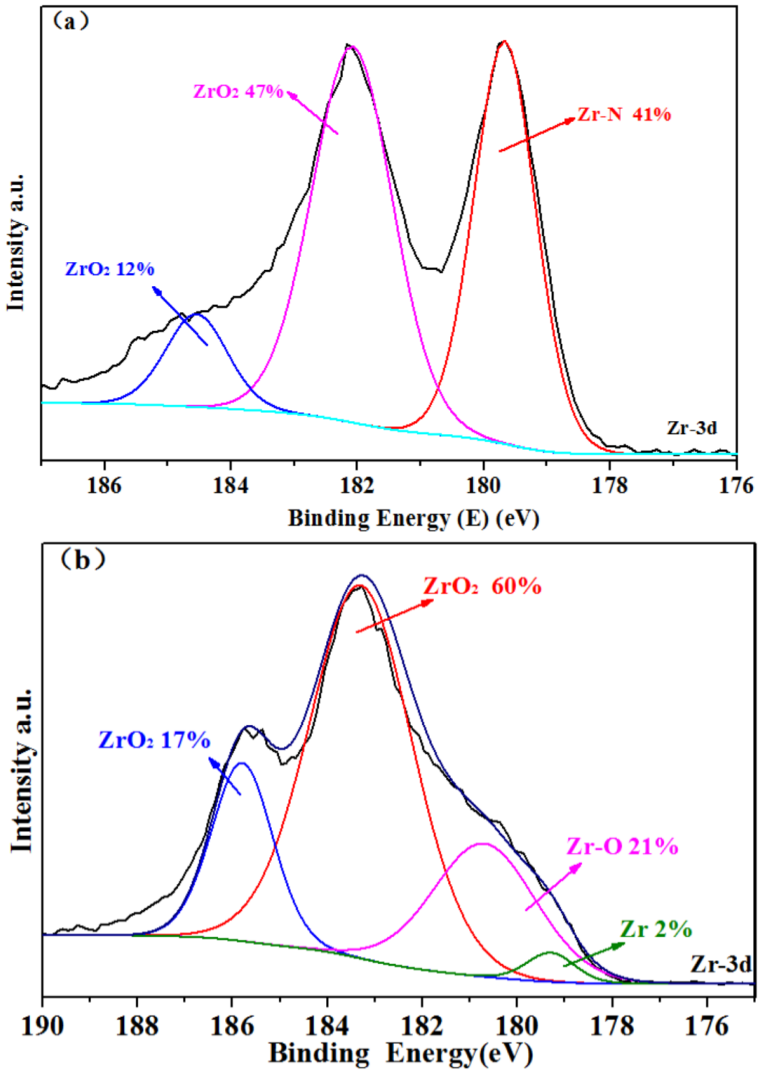

Fig.3. XPS spectra of Zr-3d from (a) surface of single layer ZrN specimen, (b) surface of bilayer ZrN/ZrO_2 specimen.

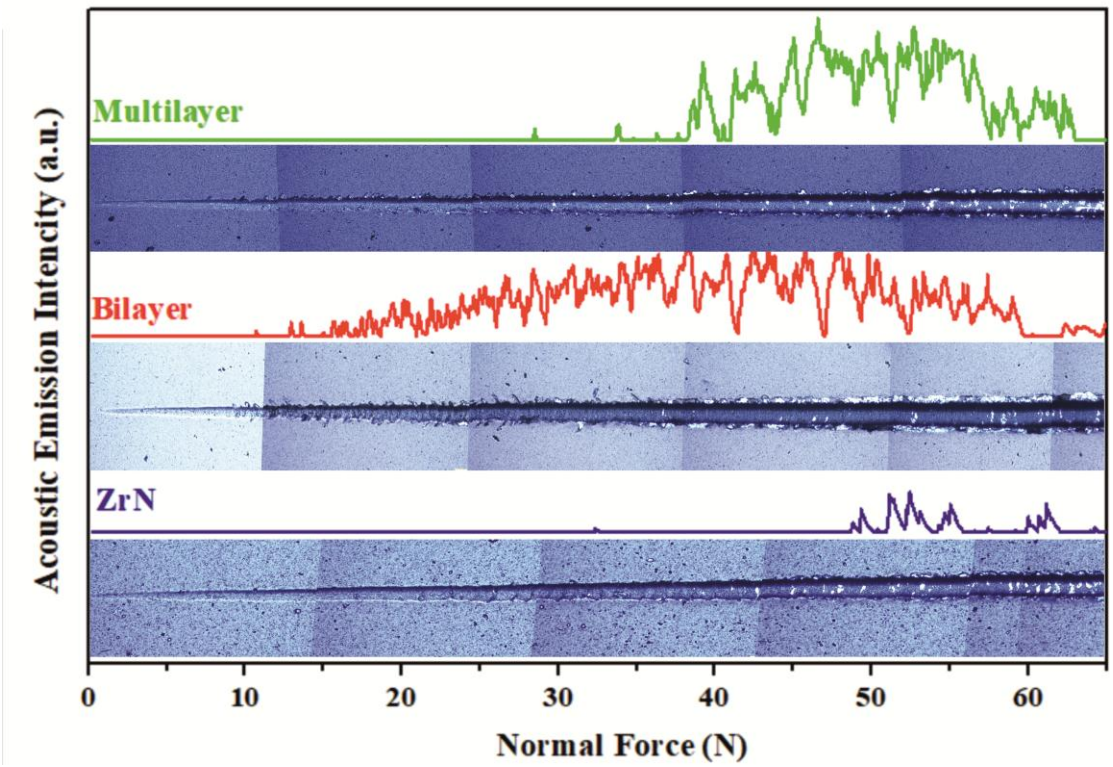

Fig.4. Acoustic emission spectra and scratch morphology of the coated specimens.

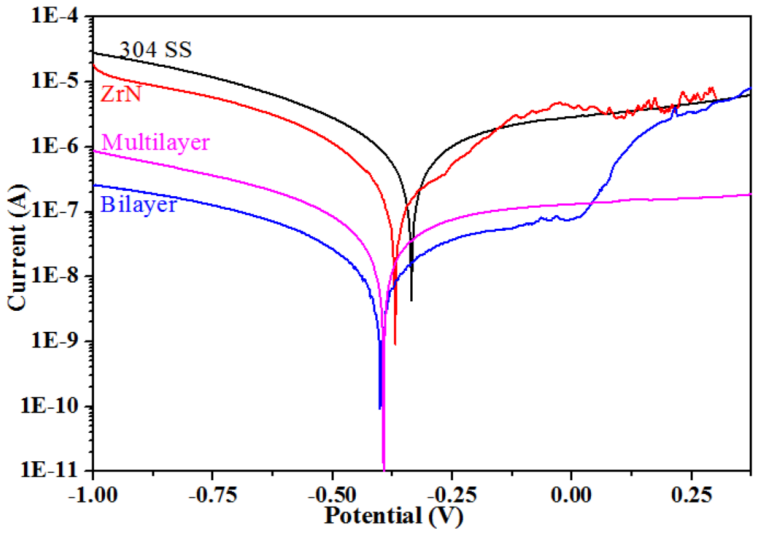

Fig.5. Potentiodynamic polarization curves for the specimens in 3.5wt% NaCl solution.

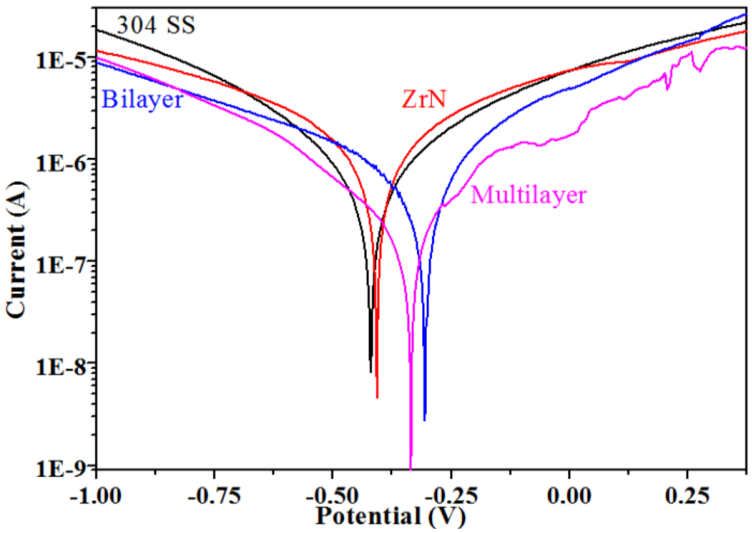

Fig.6. Potentiodynamic polarization curves for the specimens in 10 wt% hydrochloric acid solution.

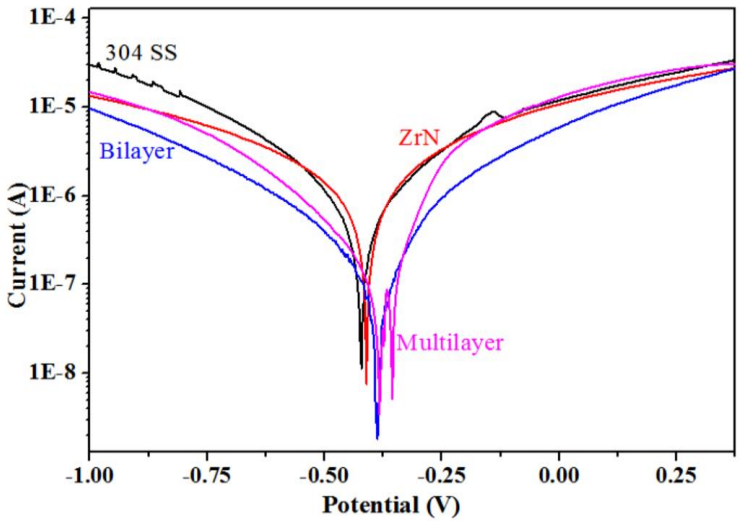

Fig.7. Potentiodynamic polarization curves for the specimens in 20 wt% hydrochloric acid solution.

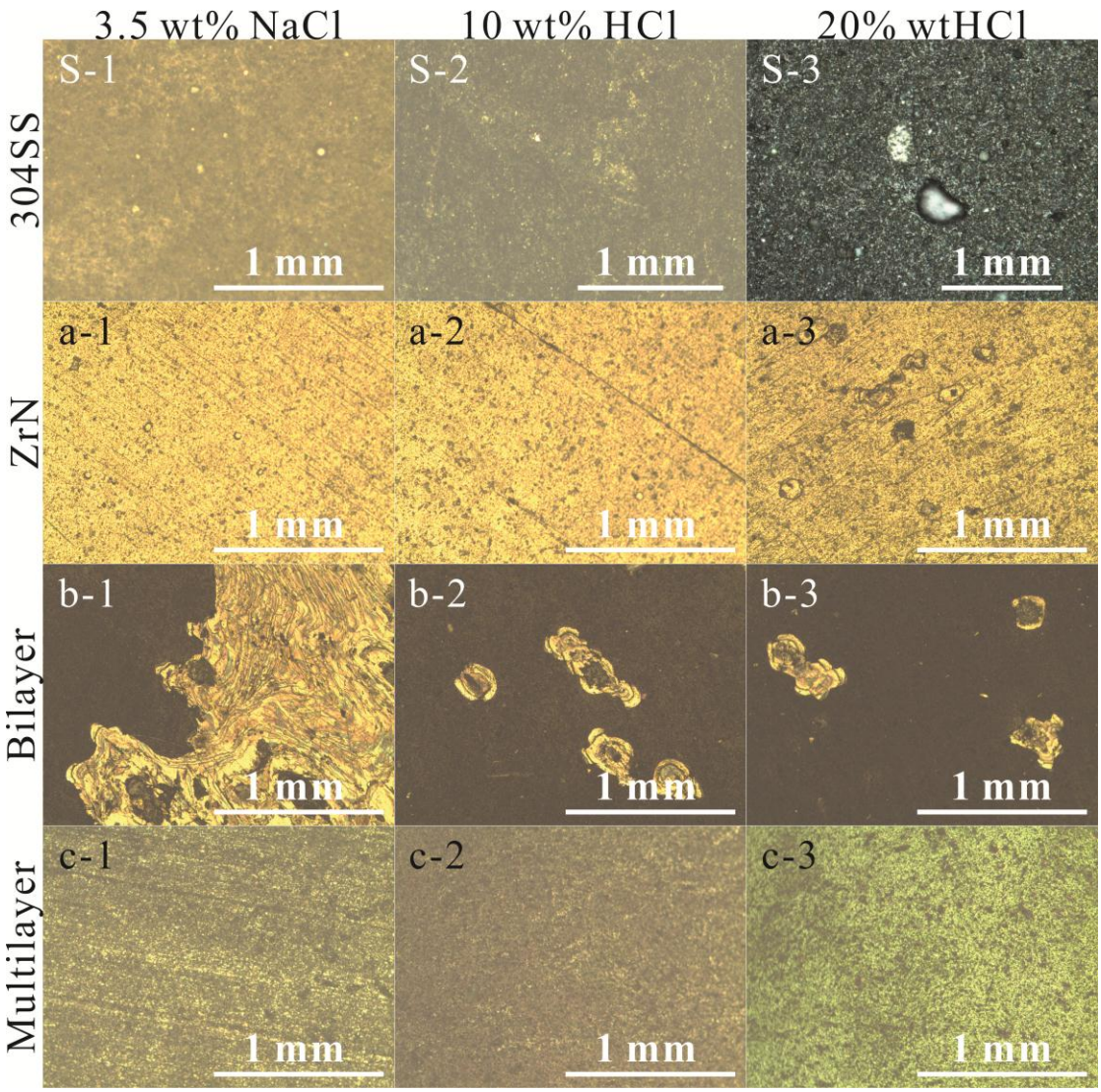

Fig.8. Surface morphology for the specimens after potentiodynamic polarization test. (S) 304 stainless steel (a) Single layer ZrN coated SS, (b) Bilayer ZrN/ZrO_2 coated SS, (c) Multilayer ZrN/ZrO_2 coated SS; (1) 3.5 wt% NaCl, (2) 10 wt% HCl, (3) 20 wt% HCl.

Table 1. Deposition details of coatings.

Specimens	Architectures	Buffer layer	Deposited time (min)	Thickness (μm)	Surface area (cm^2)
ZrN	single layer	Ti-Al	60	4.8	1
ZrN/ZrO_2 bilayer	bilayer	Ti-Al	40+50	7.0	1
ZrN/ZrO_2 multilayer	multilayer	Ti-Al	(5+5)×9	6.2	1

Table 2. Results of the corrosion test.

Specimens	3.5wt%(0.61mol/L) NaCl		10 wt% (2.87mol/L) HCl		20 wt% (6.02mol/L) HCl	
	E_{corr} (V)	I_{corr} ($A \cdot cm^{-2}$)	E_{corr} (V)	I_{corr} ($A \cdot cm^{-2}$)	E_{corr} (V)	I_{corr} ($A \cdot cm^{-2}$)
304 SS	-0.335	3.2×10^{-7}	-0.420	3.1×10^{-7}	-0.42	2.2×10^{-7}
ZrN	-0.369	1.4×10^{-7}	-0.407	3.2×10^{-7}	-0.41	3.0×10^{-7}
Bilayer	-0.401	4.2×10^{-9}	-0.306	1.04×10^{-7}	-0.387	5.4×10^{-8}
Multilayer	-0.392	1.7×10^{-8}	-0.335	8.2×10^{-8}	①-0.382	①$6.1\times10^{-8}$